Chapter 6

Magnetic and Dielectric Studies

A detailed study of the magnetic and dielectric properties of the samples has been presented in this chapter. The effect of the dopants on the magnetic behaviour of the samples has been discussed here. In order to probe the multiferroic behavior of the samples, dielectric measurements have also been performed and analyzed in an identical temperature range.

6.1 Magnetic Properties of $CuFeO_2$ and $CuFe_{0.96}Ti_{0.03}V_{0.01}O_2$ samples

A squid magnetometer (quantum design) was used to estimate and understand the magnetic properties of $CuFeO_2$ and $CuFe_{0.96}Ti_{0.03}V_{0.01}O_2$ samples. Temperature-dependent magnetic susceptibility (χ) with zero-field cooling (ZFC) was measured between 25 K and 300 K under the applied magnetic field of 5 kOe for both the samples as shown in figures 6.1 (a) and 6.1 (b).

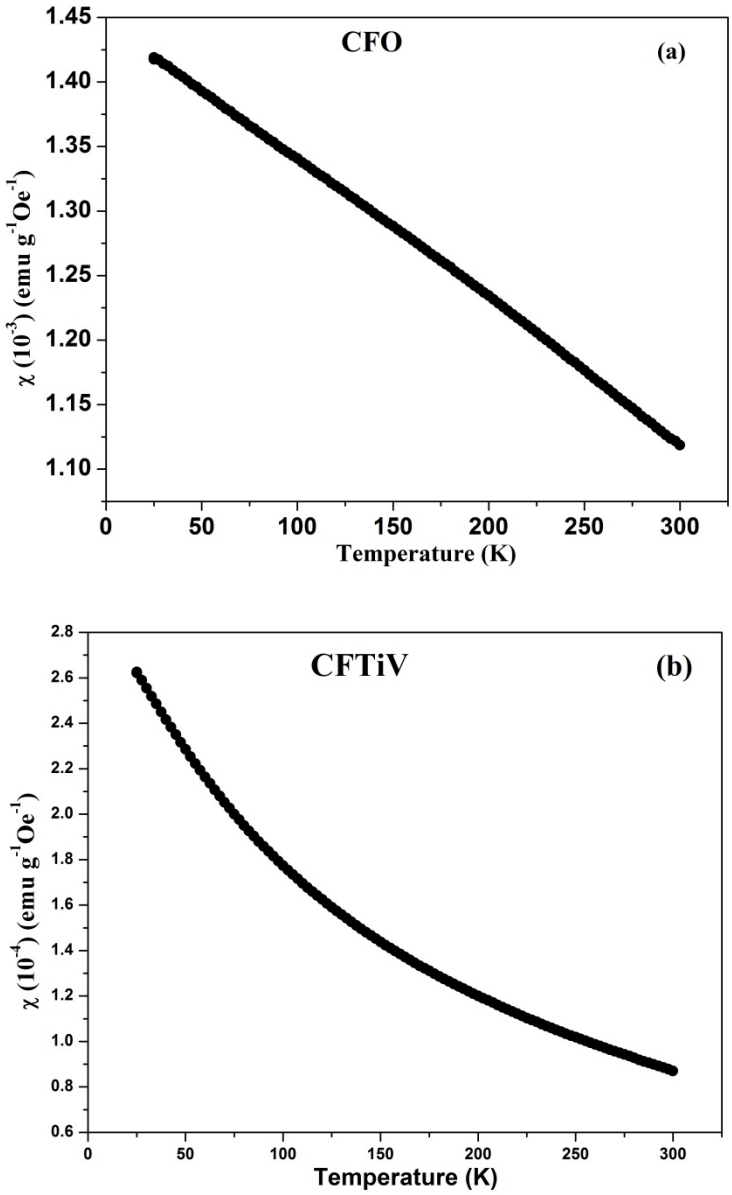

Figure 6.1: Temperature dependence of magnetic susceptibility of (a) $CuFeO_2$ and (b) $CuFe_{0.96}Ti_{0.03}V_{0.01}O_2$

χ^{-1} as a function of temperature for both the samples is shown in figures 6.2 (a) and 6.2 (b). The fitting of the Curie–Wess law [$\chi = C/(T-\theta)$] is shown with the red solid lines within the

measured temperature range. Here C and θ are the Curie-Weiss constant and Curie temperature respectively. A deviation in the *1/χ vs T* curve is observed around temperature T_o marked by arrows, which indicates the magnetic transition from paramagnetic to spin-liquid phase at this temperature as proposed earlier [1,2]. The drop in T_o in the Ti-doped sample is attributed to the role of induced local structural distortions which leads to the changes in temperature at which the release of spin frustration takes place.

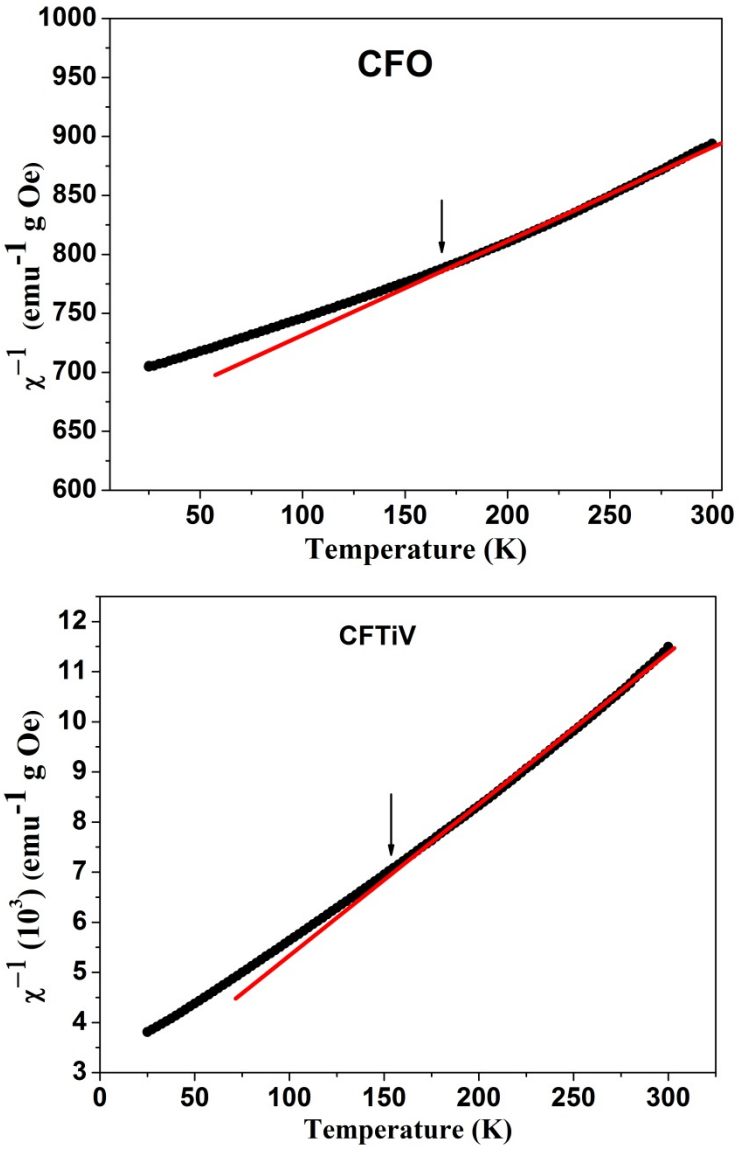

Figure 6.2: Temperature dependence of χ^{-1} along with Curie-Weiss fit for (a) $CuFeO_2$ and (b) $CuFe_{0.96}Ti_{0.03}V_{0.01}O_2$

The fitting of the Curie-Weiss law gives the values of C and θ given in table 6.1. The negative values of θ indicate the dominant antiferromagnetic interaction in the samples. A substantial decrease in the θ value for Ti-doped sample indicates the weakening antiferromagnetic interactions induced due to resultant Jahn-Teller distortions in the doped

sample. Also, the change in C values with Ti doping also can be attributed to the magnetic dilution effect, which can again be observed in the decrease of χ values with Ti doping.

Table 6. 1: Magentic properties of CFO and CFTiV samples.

Sample	C (emu K g^{-1})	θ (K)
$CuFeO_2$	1.37	-912.49
$CuFe_{0.96}Ti_{0.03}V_{0.01}O_2$	0.036	-80.45

Figures 6.3 (a) and 6.3 (b) represent the variation of isothermal magnetization with respect to the applied magnetic field ($0 \leq H \leq 70$ kOe) at 25 K, 40 K and 150 K for $CuFeO_2$ and $CuFe_{0.96}Ti_{0.03}V_{0.01}O_2$ samples. From the plot**,** it can be clearly seen that there is a sharp rise in the values of magnetization for the pristine sample at low applied fields, while there is a linear increase in magnetization values for the Ti-doped sample. Even at the highest applied field**,** no saturation magnetization is observed for the samples. Thus, it points out the further weakening of the magnetic interaction due to Ti doping at the Fe site and can be attributed to the changes in the degree of frustration induced by the enhanced local Jahn-Teller distortions, strengthening our earlier observed results on the samples using Raman and Mossbauer spectra.

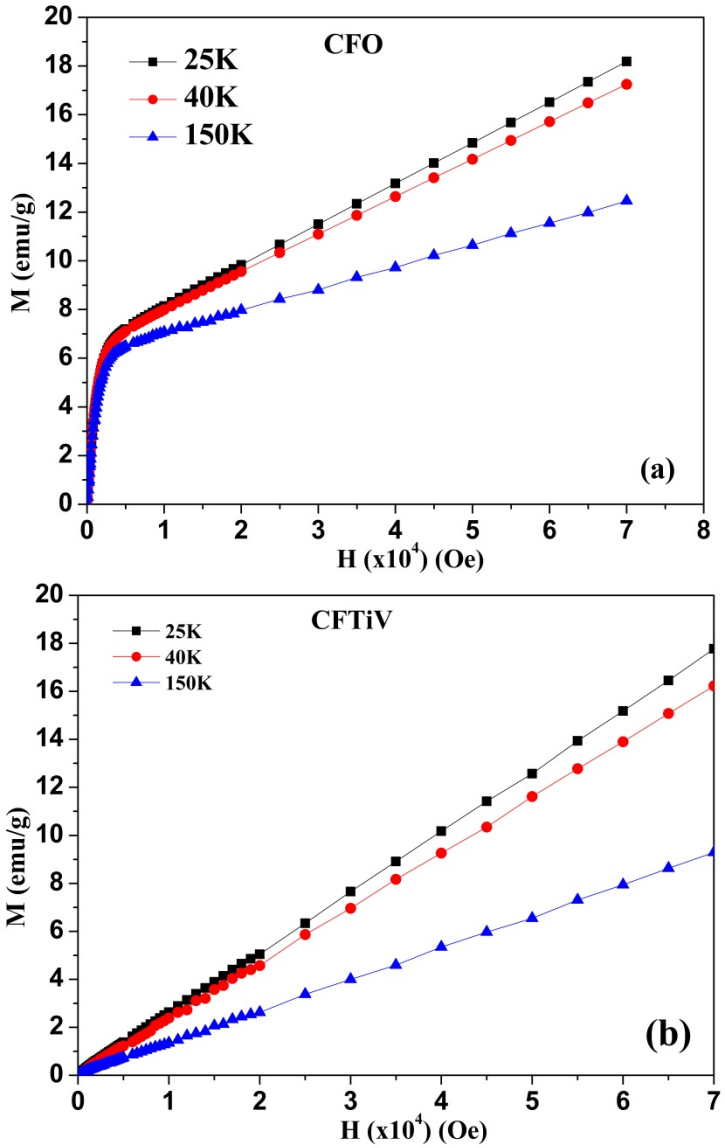

Figure 6.3: Isothermal magnetization vs applied magnetic field plots at 25 K, 40 K and 150 K for (a) $CuFeO_2$ and (b) $CuFe_{0.96}Ti_{0.03}V_{0.01}O_2$

Also adding to the above explanations, the super-exchange mechanism, Ti^{4+}-O^{2}-Ti^{4+} and Fe^{3+}-O^{2}-Ti^{4+}, as pointed out earlier can also be considered. This kind of interaction can lead to antiferromagnetic coupling reported earlier for ABO_3 type perovskite materials [3,4]. Thus Ti^{4+}substitutions at the Fe^{3+} site lead to the decrease like nearest neighbors magnetic interaction. Also, the interaction Fe^{3+}-O^{2}-Ti^{4+} is thought to be antiferromagnetic interaction and also weaker than that of Fe^{3+}-O^{2}-Fe^{3+}. Because of the limitations in the available temperature range, magnetic measurements could not be performed to observe the phase transition T_c, but strong evidence of doping-induced changes in magnetic parameters θ and T_0 (K). Here we would like to point out that the observed changes are purely due to the type of

variety of dopants selected in the present correlation-based study, even though the effect of some of the individual elements is reported before.

6.2 Dielectric properties of $CuFeO_2$ and $CuFe_{0.96}Ti_{0.03}V_{0.01}O_2$ samples

The dielectric measurements were carried out, without any temperature limitations, between room temperature and 5 K. The temperature dependence of dielectric permittivity (ε') and the corresponding dielectric loss (ε'') at different frequencies is shown in figure 6.4 for $CuFeO_2$ sample within the temperature range of 5 K to 300 K. From the plot of ε' vs T (K), it can be clearly observed that the values of ε' are found to increase sharply with an increase in temperature along with a significant effect of frequency. Also, within the same temperature regime, a maximum value in ε'' is also been observed which shifts towards the higher temperature side with increasing frequency. The temperature at which the maxima in ε'' is observed corresponds to the temperature region where a maximum dispersion in ε' values is also been detected. This kind of relationship between the ε' and the Neel temperature is consistent with the earlier reported results [5]. The Landau-Devonshire theory of phase transition in magneto-electrically ordered systems describes such magneto-electric coupling behavior whose concluding evidence is seen in our findings for the $CuFeO_2$ sample [6,7].

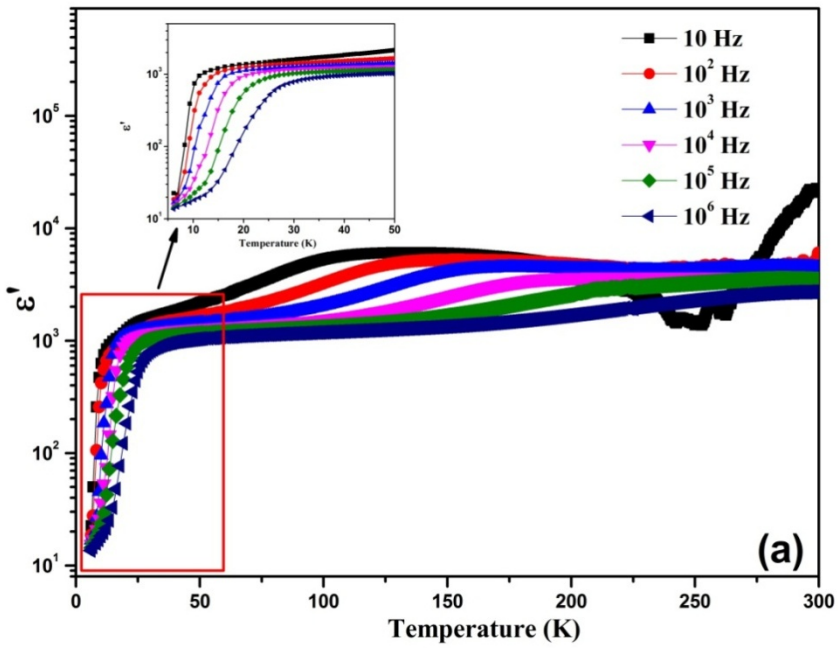

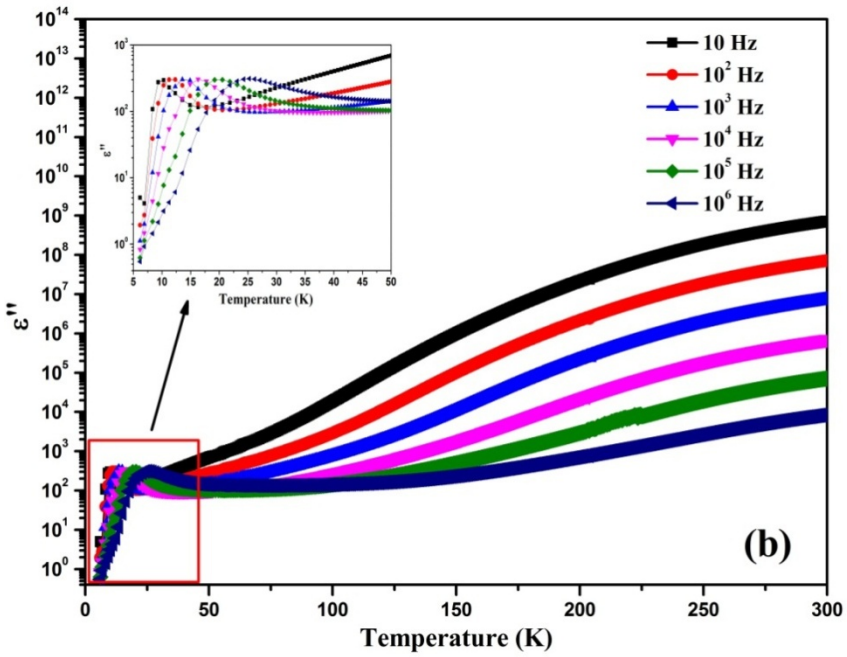

Figure 6.4: Temperature dependence of (a) ε' and (b) ε'' of ac dielectric permittivity at different frequencies for the $CuFeO_2$ sample. The insets of the figures show the variations of the real and imaginary part of ε in the temperature range of 5–50 K.

The variation of dielectric permittivity (ε') and the corresponding dielectric loss (ε'') with respect to temperature at different frequencies is represented in figure 6.5 for $CuFe_{0.96}Ti_{0.03}V_{0.01}O_2$ sample within the temperature range of 5 K to 300 K at different frequencies. From the plots, it is clear that the dielectric ordering around 15 K becomes weaker due to the Ti^{4+} doping at the Fe^{3+} site. This could also result in correlatedweakening of the magnetic ordering in the doped samples, discussed earlier. A dielectric relaxation behavior is also observed in the temperature range of 80-190 K. This behavior is independent of the magnetic ordering and also distinct compared to pure $CuFeO_2$ samples. It also follows Arrhenius law which can be seen in the inset of figure 6.5 (b). The activation energy obtained for dielectric relaxation from the fitted straight line is E_a = 0.15 eV. Low values of activation energy can be ascribed to the interplay among the lattice and polaronic defects like oxygen vacancies [8–10].

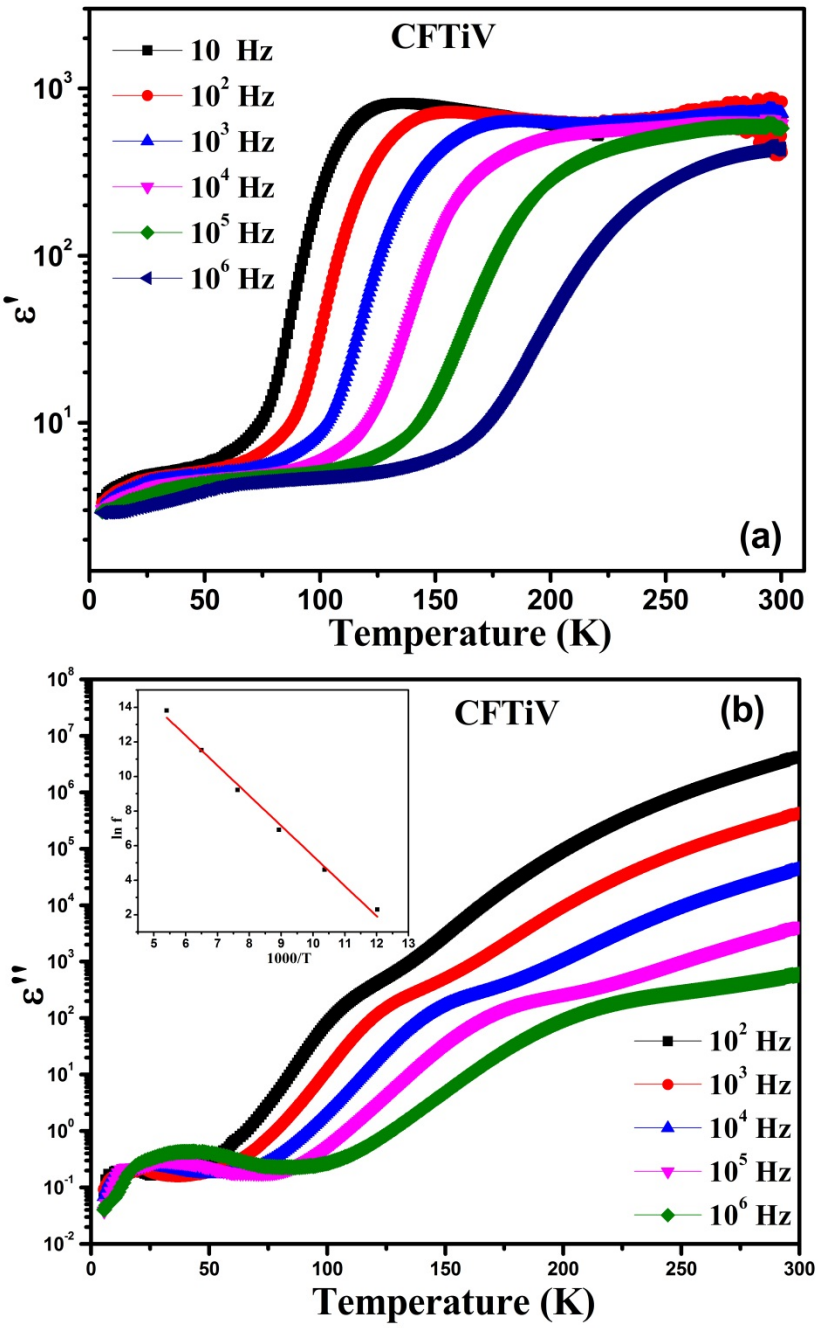

Figure 6.5: Temperature dependence of (a) ε' and (b) ε'' of ac dielectric permittivity at different frequencies for the $CuFe_{0.96}Ti_{0.03}V_{0.01}O_2$ sample. The inset of figure (b) shows the fitting of the Arrhenius law

6.3 Magnetic properties of pure and doped $CuCrO_2$ samples

The temperature-dependence of magnetic susceptibility (χ) of the pristine and doped $CuCrO_2$ isshown in figures 6.6 and 6.7, with zero-field cooling (ZFC) and field cooled (FC) conditions. The available temperature range was 25-300 K, with applied magnetic fields of 100 Oe, 5 kOe and 10 kOe. It is clear that all the samples are paramagnetic in nature above 140 K. Further, it was observed that the magnetic behavior of $CuCrO_2$ is very sensitive to the

valence state of dopants. The value of magnetization gradually saturates at around 25 K, owing to its ferromagnetic nature.

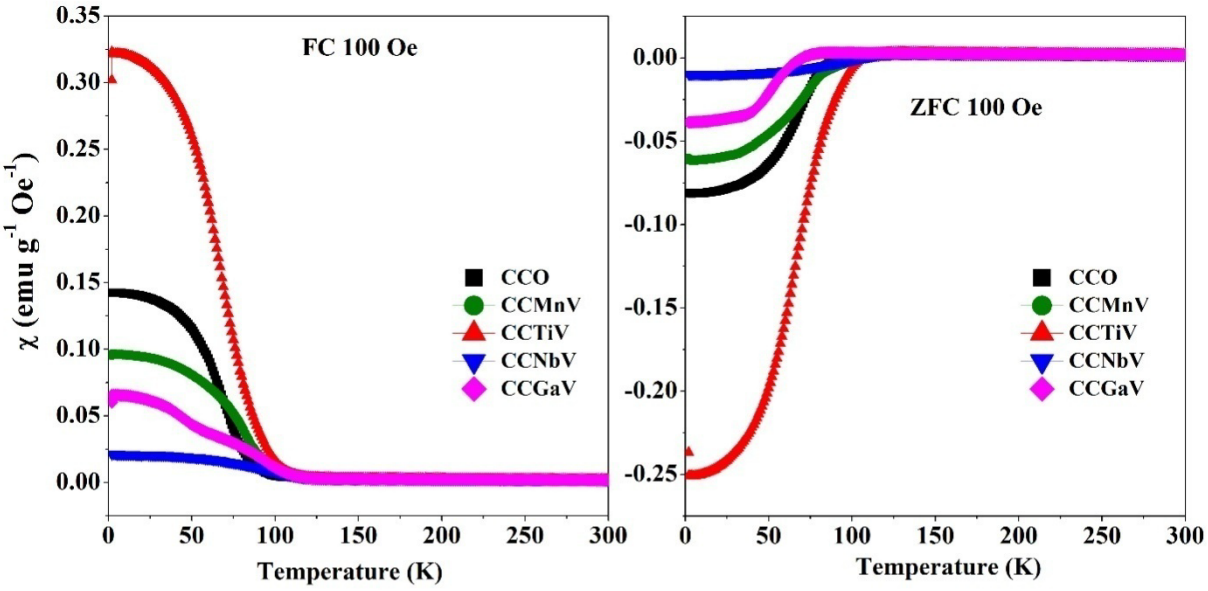

Figure 6.6: Temperature dependence of magnetic susceptibility of $CuCr_{0.96}M_{0.03}V_{0.01}O_2$ (M = Mn, Ti, Nb, and Ga) samples under 100 Oe Magnetic Field.

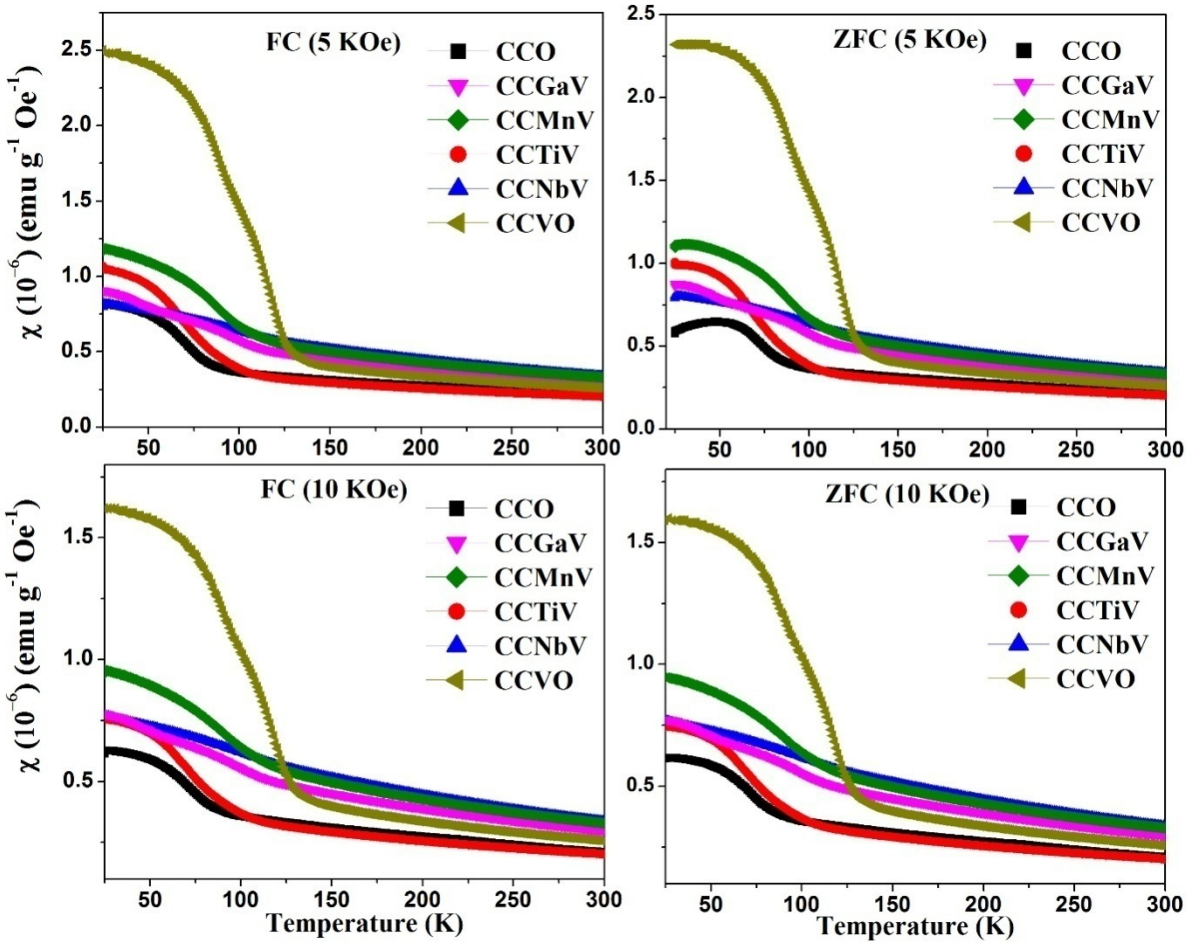

Figure 6.7: Temperature dependence of magnetic susceptibility, $CuCr_{0.96}M_{0.03}V_{0.01}O_2$ (M = Ti, Nb, Ga, and Mn), and $CuCr_{0.96}V_{0.04}O_2$ samples under two magnetic fields 5 KOe and 10 KOe.

A rather weak temperature-dependent variation of magnetic susceptibility is noticed in the Ga^{3+} and Nb^{5+} doped samples. This could be due to the closed outermost shell ($3d^{10}$ and $4p^6$, respectively), leading to their low spin configurations (S = 0). On the other hand, an abrupt increase in magnetic susceptibility appears around T_C ~110 K in the Mn/Ti-doped samples and at ~135 K for V-doped samples. Each of these ions has a partially filled outermost 3*d*/5*d* shell. The observed feature indicates the existence of the ferromagnetic (FM) interactions, ascribed to the increase in phonon-mediated spin-spin interaction.

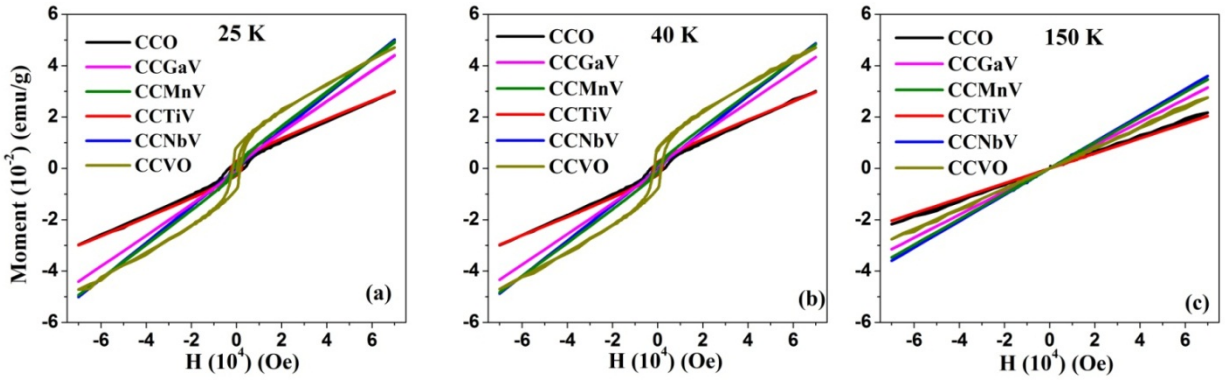

Figure 6.8: Measured M-H hysteresis curves for $CuCrO_2$, $CuCr_{0.96}M_{0.03}V0_{.01}O_2$ (M = Ti, Nb, Ga,and Mn), and $CuCr_{0.96}V_{0.04}O_2$ samples at (a) 25 K, (b) 40 K and (c) 150 K.

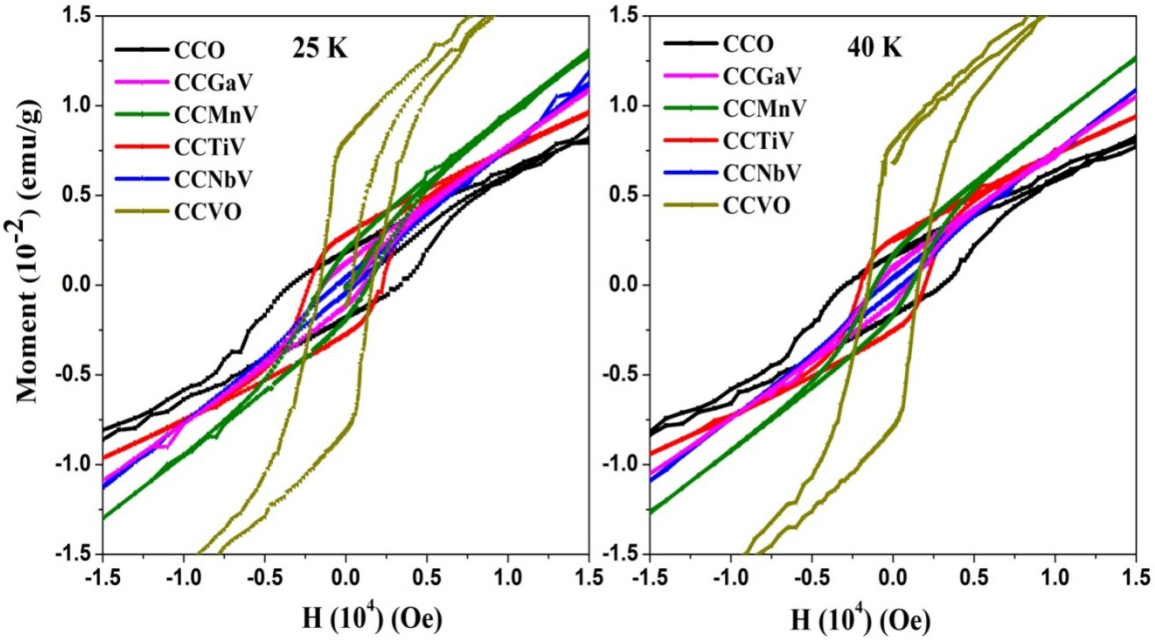

Figure 6.9: Magnified M-H hysteresis curves for $CuCrO_2$, $CuCr_{0.96}M_{0.03}V_{0.01}O_2$ (M = Ti, Nb, Ga,andMn), and $CuCr_{0.96}V_{0.04}O_2$ samples at (a) 25 K and (b) 40 K.

Table 6.2: Coercivity and Remanencemagnetization for $CuCrO_2$, $CuCr_{0.96}M_{0.03}V_{0.01}O_2$ (M = Ti, Nb, Ga, and Mn), and $CuCr_{0.96}V_{0.04}O_2$ samples at (a) 25 K and (b) 40 K.

			25 K			
Sample	CCO	CCTiV	CCNbV	CCGaV	CCMnV	CCVO
Coercivity (Oe) H_C	3400	2200	600	1400	1500	1600
Remanence Magnetization (10^{-3}) (emu/g)	1.84	2.78	0.4	1.22	1.96	8.11
			40 K			
Sample	CCO	CCTiV	CCNbV	CCGaV	CCMnV	CCVO
Coercivity (Oe)	3000	2000	600	980	1150	1500
Remanence Magnetization (10^{-3}) (emu/g)	1.66	2.55	0.39	1.02	1.68	7.92

To further investigate the magnetic behavior of these samples, we measured the *M-H* hysteresis loop, as shown in figures 6.8 and 6.9 at 25 K, 40 K, and 150 K. The measurements clearly suggest the presence of a weak FM ordering in these materials at low temperatures (≤40K), figures 6.7 (a) and (b)), but are paramagnetic at higher temperatures (≥ 120K,figure 6.7 (c)). The values ofCoercivity and Remnant magnetization for the studied samples are listed in table 6.2, which exhibit a significant variation in parameters for the V, Ti, and Mn-doped samples. None of the presently investigated samples showed saturation of magnetization under applied fields. Earlier studies also observed low-temperature ferromagnetism with no saturation magnetization [11–17] in $CuCr_{1-x}M_xO_2$, where M=Mg, Al, Sc, Mn, Fe, Co, Ga, and Rh,withcomparable *x* values as in our present work. However,none of these previous reportsobserved any significant change in the values of Coercivity and Remnant magnetization, suggesting the significance of our observations.

Various models have been proposedfor the observed ferromagnetic interaction in the $CuCr_{1-x}M_xO_2$ system at low temperatures, such as the dilution of predominantly antiferromagnetic chromium lattice [18], the free carrier-mediated double exchange mechanism [11],and hole-mediated Fe^{3+}- Cr^{3+}superexchange interactions [19]. The local spin fluctuations at the Cr^{3+}site coupled with doped itinerant holesmay break the residual magnetic degeneracy [18–

20]. The observed local disorder at the MO_6 octahedral sites accompanied by observed significant changes in the magnetic parameters (table 6.2) suggests the strong possibility of the existence of double exchange along withthe Cr-O-M-O linkages or superexchange between $M^{3+/4+}$-Cr^{3+} mediated via oxygen [21]. In particular, doping of 4+ ions, such as Ti and V, shows significant changes in the magnetic parameters. The doping of high valence ions does enhance electrical resistivity drastically, as shown earlier (figure 5.7). We have reported previously that a significant reduction in helical disorder in the vanadium doped $CuCrO_2$ samples takes place as compared to other dopants [22]. Optimization of phonon-mediated carrier-induced spin-spin interactions at low temperatures must play a curial role in the modification of the magnetic parameters, which warrants further investigation by varying valence and charge densityforsuitable ions. The advantage of mono/double doping,similar to the present work,can also be extended for further clarification. In addition to the magnetic order, these compounds also show multiferroic behavior [21,23–25].

6.4 Dielectric properties of pure and doped $CuCrO_2$ samples

The multiferroic $CuCrO_2$ was previously shown to exhibit a dielectric peak at ~25 K [23]. This finding motivated us to carry out the dielectric permittivity(ε')measurements as a function of temperature for the confirmation of magneto-dielectric coupling. As shown in figures 6.9 and 6.10, a clear indication of the magneto-dielectric coupling in the pristine and doped samples is observed. The Nb and V doped samples exhibit a peak in dielectric permittivity at nearly the same temperature. Earlier we have reported comparatively less local distortion in Nb^{5+} and V^{5+} doped samples during Raman studies [22], and their ionic sizes are also almost the samebut smaller than that of Cr^{3+}, which results in the weakening of the distortion of the MO_6 octahedra. Therefore, there might be a negligible change in the metal-ligand hybridization-based spin-spin coupling, and the ferroelectric polarization temperature [26].

In the case of Mn, Ti, and Fe doped samples,a strong local distortion was observed in Raman spectra [22],presumably due to the substantial Jahn-Teller distortions surrounding the Cr site [26–29]. This may be responsible for the broadening and shifting of the peak in dielectric permittivity towards lower temperatures. It is noticed that the Ni and Fe doped sampleshave a weaker temperature variation inε' as well as a shift of singularity towards the lower temperatures. These findings are correlated with the much higherelectrical conductivity of these samples as compared to other samples.

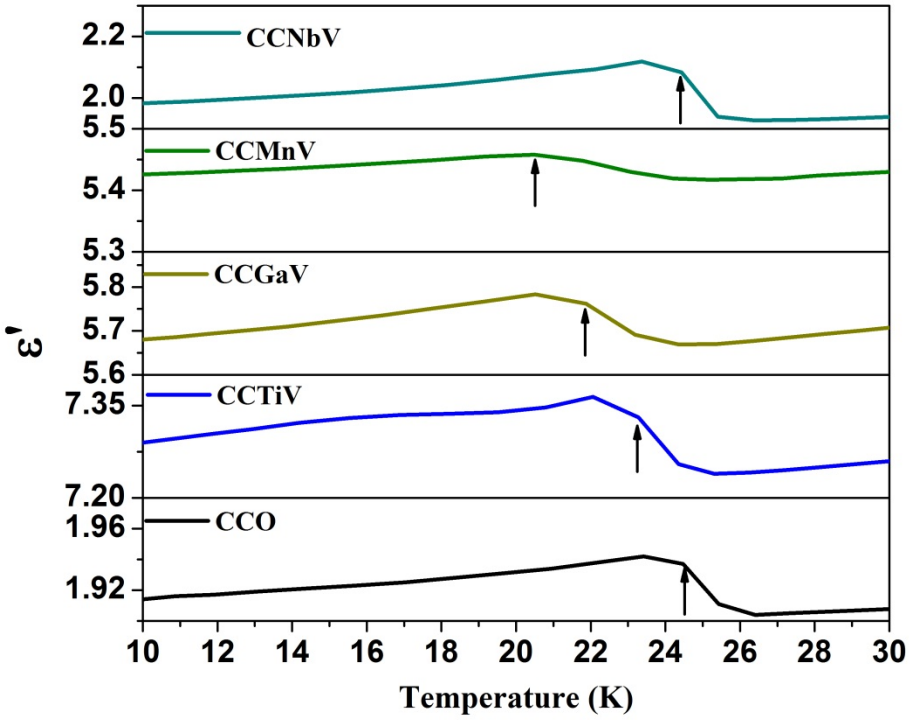

Figure 6.10: Temperature-dependent dielectric constant of $CuCrO_2$ and $CuCr_{0.96}M_{0.03}V_{0.01}O_2$ (M = Ti, Mn, Ga, and Nb) samples.

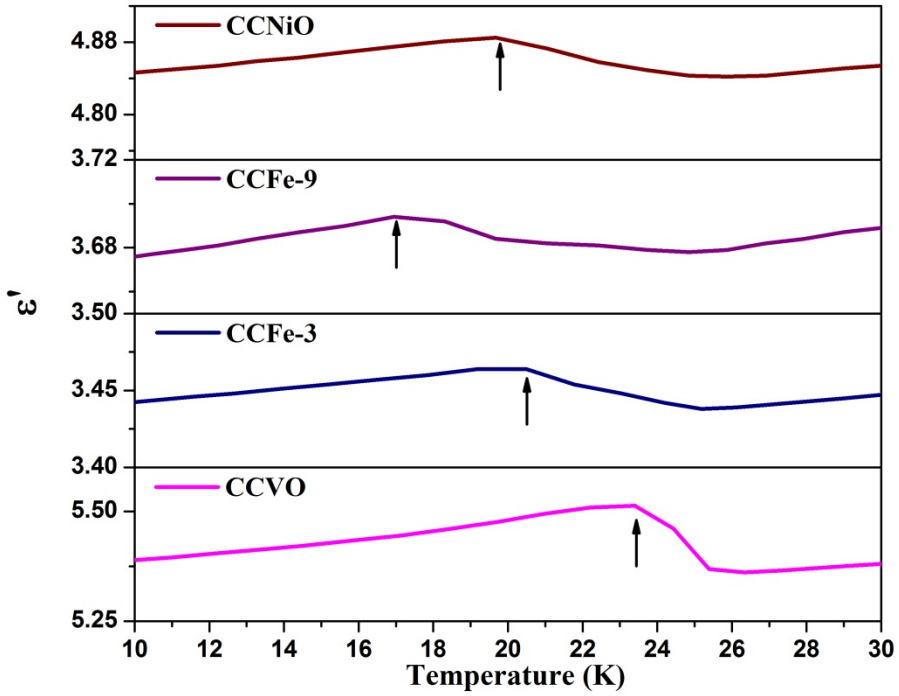

Figure 6.11: Temperature-dependent dielectric constant of $CuCr_{1-x}Fe_xO_2$ (x = 0.03and 0.09), $CuCr_{0.97}Ni_{0.03}O_2$, and $CuCr_{0.96}V_{0.04}O_2$ samples.

6.5 Conclusions

Following conclusions can be drawn from the above studies:

- For the $CuFeO_2$ system, the Jahn–Teller effect-based local defects play an significant role in the magnetic and dielectric properties of the Ti-doped sample, predominantly at low temperatures and/or at low applied magnetic fields. Furthermore, the present correlated study evidently highlights the role of doping level and local distortions in determining the magnetic and multiferroic nature of this system providing an effective tool to tune its chemical and physical behavior.
- For the $CuCrO_2$ system, the optimization of the phonon-induced localized carrier hole density along with the reduction in helical disorder around MO_6 octahedra through suitable electron/hole doping is an effective way to enhance the double exchange along with the Cr-O-M-O linkages or superexchange between $M^{3+/4+}$-Cr^{3+} mediated by oxygen at low temperatures. Clear evidence of the magneto-dielectric coupling in all studied sampleshave been observed from the magnetization and dielectric permittivity measurements.

References

[1] K. Hayashi, T. Nozaki, R. Fukatsu, Y. Miyazaki, T. Kajitani, Spin dynamics of triangular lattice antiferromagnet $CuFeO_2$: Crossover from spin-liquid to paramagnetic phase, Phys. Rev. B - Condens. Matter Mater. Phys. 80 (2009). https://doi.org/10.1103/PhysRevB.80.144413.

[2] S.Y. Wu, W.H. Li, C.C. Yang, J.W. Lynn, R.S. Liu, Magnetic ordering of Mn and Ru in $(La_{0.52}Ba_{0.48})(Mn_{0.51}Ru_{0.49})O_3$, Phys. Status Solidi Basic Res. 244 (2007) 2233–2241. https://doi.org/10.1002/pssb.200642028.

[3] S. Sen, N. Chakraborty, P. Rana, R. Sahu, S. Singh, A.K. Panda, S. Tripathy, D.K. Pradhan, A. Sen, Effect of Ti doping on the structural, electrical and magnetic properties of $GaFeO_3$, J. Mater. Sci. Mater. Electron. 27 (2016) 4647–4652. https://doi.org/10.1007/S10854-016-4342-7/TABLES/2.

[4] N.O. Khalifa, H.M. Widatallah, A.M. Gismelseed, F.N. Al-Mabsali, R.G. S. Sofin, M. Pekala, Magnetic and Mössbauer studies of pure and Ti-doped $YFeO_3$ nanocrystalline particles prepared by mechanical milling and subsequent sintering, Hyperfine Interact. 2016 2371. 237 (2016) 1–11. https://doi.org/10.1007/S10751-016-1287-4.

[5] M. Polomska, W. Kaczmarek, Z. Pająk, Electric and magnetic properties of $(B_{1-x}La_x)FeO_3$ solid solutions, Phys. Status Solidi. 23 (1974) 567–574. https://doi.org/10.1002/PSSA.2210230228.

[6] V.R. Palkar, D.C. Kundaliya, S.K. Malik, S. Bhattacharya, Magnetoelectricity at room temperature in the $Bi_{0.9-x}Tb_xFeO_3$ system, Phys. Rev. B - Condens. Matter Mater. Phys. 69 (2004). https://doi.org/10.1103/PhysRevB.69.212102.

[7] K.C. Verma, R.K. Kotnala, Tailoring the multiferroic behavior in $BiFeO_3$ nanostructures by Pb doping, RSC Adv. 6 (2016) 57727–57738. https://doi.org/10.1039/c6ra12949h.

[8] S. Mukherjee, R. Gupta, A. Garg, Dielectric response and magnetoelectric coupling in single crystal gallium ferrite, AIP Adv. 3 (2013). https://doi.org/10.1063/1.4806762.

[9] C.C. Wang, L.W. Zhang, Polaron relaxation related to localized charge carriers in $CaCu_3Ti_4O_{12}$, Appl. Phys. Lett. 90 (2007). https://doi.org/10.1063/1.2719608.

[10] V. Singh, A. Daryapurkar, S.S. Rajput, S. Mukherjee, A. Garg, R. Gupta, Effect of annealing atmosphere on leakage and dielectric characteristics of multiferroic gallium ferrite, J. Am. Ceram. Soc. 100 (2017) 5226–5238. https://doi.org/10.1111/jace.15053.

[11] D. Li, X. Fang, W. Dong, Z. Deng, R. Tao, S. Zhou, J. Wang, T. Wang, Y. Zhao, X. Zhu, Magnetic and electrical properties of p-type Mn-doped $CuCrO_2$ semiconductors, J. Phys. D. Appl. Phys. 42 (2009). https://doi.org/10.1088/0022-3727/42/5/055009.

[12] F. Lin, W. Shi, A. Liu, Optical bandgap modulation and magnetic characterization of Fe-doped $CuCrO_2$ nanopowders, J. Alloys Compd. 529 (2012) 21–24. https://doi.org/10.1016/j.jallcom.2012.03.059.

[13] T. Elkhouni, M. Amami, C. V. Colin, P. Strobel, A. Ben Salah, The structure, Raman spectroscopy and evidence of ferromagnetic transition in $CuCr_{1-x}MxO_2$ (M=Mn and Rh) compounds, J. Magn. Magn. Mater. 355 (2014) 158–163. https://doi.org/10.1016/J.JMMM.2013.12.004.

[14] T. Elkhouni, M. Amami, C. V. Colin, P. Strobel, A. Ben Salah, Synthesis, structural and magnetic studies of the $CuCr_{1-x}Co_xO_2$ delafossite oxide, J. Magn. Magn. Mater. 330 (2013) 101–105. https://doi.org/10.1016/J.JMMM.2012.10.037.

[15] T. Elkhouni, M. Amami, P. Strobel, A. Ben Salah, Structural and Magnetic Properties of Substituted Delafossite-Type Oxides $CuCrO_2$, World J. Condens. Matter Phys. 03 (2013) 1–8. https://doi.org/10.4236/wjcmp.2013.31001.

[16] A. Maignan, C. Martin, R. Frésard, V. Eyert, E. Guilmeau, S. Hébert, M. Poienar, D. Pelloquin, On the strong impact of doping in the triangular antiferromagnet $CuCrO_2$, Solid State Commun. 149 (2009) 962–967. https://doi.org/10.1016/j.ssc.2009.02.026.

[17] F. Jlaiel, M. Amami, N. Boudjada, P. Strobel, A. Ben Salah, Metal transition doping effect on the structural and physical properties of delafossite-type oxide $CuCrO_2$, J. Alloys Compd. 509 (2011) 7784–7788. https://doi.org/10.1016/J.JALLCOM.2011.04.153.

[18] M. Poienar, F. Damay, C. Martin, V. Hardy, A. Maignan, G. André, Structural and magnetic properties of $CuCr_{1-x}Mg_xO_2$ by neutron powder diffraction, Phys. Rev. B - Condens. Matter Mater. Phys. 79 (2009). https://doi.org/10.1103/PhysRevB.79.014412.

[19] C. Gao, F. Lin, X. Zhou, W. Shi, A. Liu, Fe concentration dependences of microstructure and magnetic properties for $Cu(Cr_{1-x}Fe_x)O_2$ ceramics, J. Alloys Compd. 565 (2013) 154–158. https://doi.org/10.1016/j.jallcom.2013.02.161.

[20] H. Yamaguchi, S. Ohtomo, S. Kimura, M. Hagiwara, K. Kimura, T. Kimura, T. Okuda, K. Kindo, Spiral-plane flop probed by ESR in the multiferroic triangular-lattice antiferromagnet $CuCrO_2$, Phys. Rev. B - Condens. Matter Mater. Phys. 81 (2010) 033104. https://doi.org/10.1103/PHYSREVB.81.033104/FIGURES/4/MEDIUM.

[21] T. Kimura, J.C. Lashley, A.P. Ramirez, Inversion-symmetry breaking in the noncollinear magnetic phase of the triangular-lattice antiferromagnet $CuFeO_2$, Phys. Rev. B - Condens. Matter Mater. Phys. 73 (2006) 1–4. https://doi.org/10.1103/PhysRevB.73.220401.

[22] N. Barot, P.K. Mehta, A. Rao, R. Thomas, Y.-K. Kuo, Effects of iso- and polyvalent substitutions on the short/long-range crystalline order in $CuCrO_2$ compounds, J. Alloys Compd. 791 (2019). https://doi.org/10.1016/j.jallcom.2019.03.291.

[23] S. Seki, Y. Onose, Y. Tokura, Spin-driven ferroelectricity in triangular lattice antiferromagnets $ACrO_2$ (A=Cu, Ag, Li, or Na), Phys. Rev. Lett. 101 (2008) 067204. https://doi.org/10.1103/PHYSREVLETT.101.067204/FIGURES/4/MEDIUM.

[24] E. Pachoud, K. Singh, Y. Bréard, C. Martin, G. André, V. Hardy, C. Simon, A. Maignan, Magnetic dilution and steric effects in the multiferroic delafossite $CuCrO_2$, Phys. Rev. B - Condens. Matter Mater. Phys. 86 (2012) 054437. https://doi.org/10.1103/PHYSREVB.86.054437/FIGURES/12/MEDIUM.

[25] A.T. Apostolov, I.N. Apostolova, S. Trimper, J.M. Wesselinowa, Dielectric properties of multiferroic $CuCrO_2$, Eur. Phys. J. B. 90 (2017). https://doi.org/10.1140/epjb/e2017-80461-4.

[26] S. Lenjer, O.F. Schirmer, H. Hesse, T.W. Kool, Conduction states in oxide perovskites: Three manifestations of (formula presented) Jahn-Teller polarons in barium titanate, Phys. Rev. B - Condens. Matter Mater. Phys. 66 (2002) 1–12. https://doi.org/10.1103/PhysRevB.66.165106.

[27] H. Yabuta, H. Tanaka, T. Furuta, T. Watanabe, M. Kubota, T. Matsuda, T. Ifuku, Y. Yoneda, Enhancement of tetragonal anisotropy and stabilisation of the tetragonal

phase by Bi/Mn-double-doping in $BaTiO_3$ ferroelectric ceramics, Sci. Rep. 7 (2017). https://doi.org/10.1038/srep45842.

[28] J. Fridrichová, P. Bačík, A. Ertl, M. Wildner, J. Dekan, M. Miglierini, Jahn-Teller distortion of Mn^{3+}-occupied octahedra in red beryl from Utah indicated by optical spectroscopy, J. Mol. Struct. 1152 (2018) 79–86. https://doi.org/10.1016/j.molstruc.2017.09.081.

[29] D.D. Shah, P.K. Mehta, M.S. Desai, C.J. Panchal, Origin of giant dielectric constant in $Ba[(Fe_{1-x}Co_x)_{1/2}Nb_{1/2}]O_3$, J. Alloys Compd. 509 (2011) 1800–1808. https://doi.org/10.1016/j.jallcom.2010.10.045.